Report No.
UCB/SEMM-2005/02

Structural Engineering
Mechanics and Materials

An Adaptive Hybrid Time-Stepping Scheme for Highly Nonlinear Strongly Coupled Problems

By

Prashanth K. Vijalapura

and

Sanjay Govindjee

February 2005

Department of Civil and Environmental Engineering
University of California, Berkeley

An Adaptive Hybrid Time-Stepping Scheme for Highly Nonlinear Strongly Coupled Problems

Prashanth K. Vijalapura[†] and Sanjay Govindjee[*]

Department of Civil & Environmental Engineering, UC Berkeley, Berkeley CA 94720

SUMMARY

This paper deals with the design and implementation of an adaptive hybrid scheme for the solution of highly nonlinear, strongly coupled problems. The term "hybrid" refers to a composite time stepping scheme where a controller decides whether a monolithic scheme or a fractional step (splitting) scheme is appropriate for a given time step. The criteria are based on accuracy and efficiency. The key contribution of this paper is the development of a framework for incorporating error criteria for stepsize selection and a mechanism for choosing from splitting or monolithic possibilities. The resulting framework is applied to silylation, a highly nonlinear, strongly coupled problem of solvent diffusion and reaction in deforming polymers. Numerical examples show the efficacy of our new hybrid scheme on both two- and three-dimensional silylation simulations in the context of microlithography.

KEY WORDS: operator splitting; fractional step methods; coupled problems; Hybrid scheme; time stepping; silylation; microlithography

1. Introduction

The numerical simulation of transient, strongly coupled systems of Partial Differential Equations (PDEs) is a well-known challenging problem. The assurance of accuracy while remaining efficient is especially difficult. For time-stepping coupled problems numerically, one can adopt the commonly used monolithic scheme which involves evolving the coupled field variables simultaneously. In contrast, one can also use the method of fractional steps (also known as operator splitting) which decouples the coupled problem and results in smaller problems which can in turn be numerically integrated in time. Both these approaches are common in the literature and for our purposes we will consider them in the context of PDEs which have already been spatially discretized. Thus, we wish to concentrate on systems of Ordinary Differential Equations (ODEs) and Differential-algebraic-equations (DAEs).

[*] Correspondence to: Prof. Sanjay Govindjee, Email: sanjay@ce.berkeley.edu
[†] Formerly, Graduate Student at UC Berkeley, Currently employed at ABAQUS Inc., Providence, RI 02909

Monolithic schemes, although straightforward from an analysis viewpoint can become inefficient as the coupled equations have to be integrated simultaneously. When implicit time stepping schemes [23] are used on ODEs arising from the spatial discretization of the coupled problem, a huge system of nonlinear algebraic equations for the coupled field variables has to be solved at each time step making it expensive. The issue of solving nonlinear algebraic equations can be avoided by using explicit time stepping schemes. However, these schemes have stepsize restrictions due to stability [41] which can be severe. Consequently, in many cases, the only viable option is to use implicit schemes [40]. Further, in the context of DAEs [7], fully explicit time stepping is not possible as nonlinear algebraic equations have to be solved at each time step to satisfy the algebraic constraints. Therefore, in the context of DAEs, fully implicit schemes are preferred (see for e.g., Refs. [15, 11, 22]). For the strongly nonlinear problems in these references, full Newton iterations have been used making the simulations expensive. It is in this context that fractional step methods are helpful. Fractional step methods decouple the coupled operator describing the coupled phenomenon by additively splitting it in such a way that smaller problems for individual phenomena result. The splitting schemes offer several advantages which include, a) computational savings from smaller problem sizes and possible symmetry in sub-problems, b) flexibility from working with smaller sized decoupled problems in terms of data storage and reusing computer codes tuned to individual sub-problems. Consequently, splitting schemes have been widely used in various applications such as, thermo-elastoplasticity[3], soil consolidation [2, 42, 36, 25, 14], silicon oxidation [10], thermo-hydromechanical problems [28], reaction transport problems [6], atmospheric sciences [24] etc. In spite of these contributions, the use of fractional step methods particularly for DAEs with extreme nonlinearities and strong coupling needs a fresh look as will be explained later.

Our motivation for considering coupled problems comes from the numerical simulation of *silylation*, a process step in microlithography [29]. Silylation involves solvent diffusion and reaction of a solvent in a polymeric photoresist [12]. The selective diffusion is effected through a crosslinking pattern created on the polymer substrate by selective exposure to UltraViolet radiation through a mask. The silylation polymer-solvent mixture that is formed in the non-crosslinked regions has altered properties making it resistant to etching while the crosslinked regions are vulnerable. This step in turn is followed by etching the vulnerable regions and subsequent development of topographical features on the polymeric photoresist in order to manufacture a microchip. Silylation involves a strong physical coupling between solvent diffusion, reaction, and polymer deformation. Solvent presence causes the polymer to undergo a glass-rubber phase transition [8]. This results in a steep drop in the relaxation times, thereby enhancing segmental re-orientation, and subsequently causes large swelling (as much as 50%). Solvent diffusion itself is strongly affected by the swelling state. The solvent piles up at a sharp interface between the wet and the dry polymer while waiting for the dry polymer to expand for additional solvent diffusion. Consequently, sharp solvent diffusion fronts are created which also move at a constant speed. These characteristics constitute Case II diffusion[27, 35, 34, 1, 16, 37], an important and well recognized regime of solvent diffusion in polymers. Our mathematical model for silylation reflects these physically strong couplings by way of extreme nonlinearities in the model's constitutive relations. Further, a realistic quasi-static assumption is made for the polymer deformation problem which is coupled to a first order mass balance equation for solvent diffusion. These coupled partial-diferential-equations (PDEs) on spatial discretization lead to a system of highly nonlinear, strongly coupled DAEs.

Time integrating these coupled, nonlinear DAEs is a significant challenge.

In the context of extreme nonlinearities, as with our silylation problem, monolithic implementations can be expensive when efficient iterative schemes like Krylov methods [21] do not perform well forcing full Newton iterations. In such cases, the expense comes from linear solves of generally unsymmetric matrices. On the other hand, using splitting as an alternative is still deficient because none of the current splitting implementations have a mechanism to control splitting errors. This crucially affects accuracy for strongly coupled problems. Therefore, in spite of their efficiency, splitting schemes have had mixed success in strongly coupled situations. Given the accuracy and efficiency concerns, it is hard to conclude whether the monolithic or the split implementation is the best choice for a particular problem. For either of the choices, if least expense needs to be ensured for a target accuracy, stepsize adaptivity is necessary. Adaptive time stepping schemes for monolithic schemes have been applied for both ODEs and DAEs in the engineering literature (see e.g., [15, 37, 31]). Similarly, monolithic equations are solved using a staggered solution procedure with iterations converging to the monolithic solution [43, 44, 36]. However, adaptive time stepping for splitting schemes hardly exists (see e.g., [6]). Even in such cases, splitting error is not explicitly controlled making them ineffective for strongly coupled problems. Moreover, the theoretical aspects of splitting techniques for DAEs has only been recently established[38]. Considering these factors, the objectives of this paper are:

1. Develop an efficient, accurate and a robust adaptive time stepping scheme for highly nonlinear, strongly coupled problems including the case of DAEs and ODEs.
2. Apply the resulting numerical scheme for validation on silylation, a strongly coupled, highly nonlinear problem of solvent diffusion and reaction in deforming polymers.

To this end, a novel, adaptive hybrid scheme is developed. Following a brief introduction to operator splitting, the complete details of the hybrid scheme and the issues it addresses are presented. This abstract presentation for general DAEs is followed by application details of silylation, our specific problem of solvent diffusion and reaction in deforming polymers. Numerical examples for silylation are presented in both 2- and 3-D settings which demonstrate that the stated objectives are met.

2. Adaptive Time Stepping Schemes

Consider a canonical system of DAEs in $\mathbf{x}$ and $\mathbf{y}$ as shown in Eqn. (1).

$$\begin{pmatrix} \mathbf{0} \\ \dot{\mathbf{y}} \end{pmatrix} = \begin{pmatrix} \mathbf{G}(\mathbf{x},\mathbf{y}) \\ \mathbf{F}(\mathbf{x},\mathbf{y}) \end{pmatrix} := \boldsymbol{\chi}. \tag{1}$$

Here $\boldsymbol{\chi}$ denotes a nonlinear operator in general. The DAEs are assumed to be of index-1 meaning that along the solution, the algebraic variables $\mathbf{x}$ can be expressed in terms of the ODE variables $\mathbf{y}$[†]. Further, $\dot{(\,)}$ denotes a time derivative. This canonical formulation provides

[†]For coupled problems involving mechanical displacements and an auxiliary field as in diffusion-deformation coupling, or thermoelasticity or consolidation-flow coupling, this assumption is equivalent to a non-restrictive condition, namely, invertibility of the stiffness matrix associated with the mechanical DOFs.

a suitable abstraction for describing the time stepping scheme in addition to simplifying the notation. The adaptive hybrid scheme which accommodates both monolithic and splitting steps is described using this canonical form.

2.1. Time Splitting/Fractional Steps

A typical monolithic step for time stepping in the time interval $[t_n, t_{n+1}]$ involves, time discretization of the ODE part of (1) and solving the resulting equations simultaneously for both $\mathbf{x}$ and $\mathbf{y}$ at t_{n+1}. In a splitting step, the evolution of the ODE variables $\mathbf{y}$ is decoupled from the solution of the algebraic variables $\mathbf{x}$. Consequently, the split equations governing the separate evolution of $\mathbf{x}$ and $\mathbf{y}$ can be written as:

$$\begin{pmatrix} \mathbf{0} \\ \dot{\mathbf{y}} \end{pmatrix} = \underbrace{\begin{pmatrix} \mathbf{G}(\mathbf{x},\mathbf{y}) \\ \mathbf{0} \end{pmatrix}}_{\boldsymbol{\chi}_1 - Algebraic} \qquad \begin{pmatrix} \dot{\mathbf{x}} \\ \dot{\mathbf{y}} \end{pmatrix} = \underbrace{\begin{pmatrix} \mathbf{0} \\ \mathbf{F}(\mathbf{x},\mathbf{y}) \end{pmatrix}}_{\boldsymbol{\chi}_2 - ODEs}, \tag{2}$$

where $\boldsymbol{\chi} = \boldsymbol{\chi}_1 + \boldsymbol{\chi}_2$. Such an additive decomposition of operators is well understood [33] in the context of pure ODEs where the split equations often take the form:

$$\underbrace{\begin{pmatrix} \dot{\mathbf{x}} \\ \dot{\mathbf{y}} \end{pmatrix} = \begin{pmatrix} \mathbf{G}(\mathbf{x},\mathbf{y}) \\ \mathbf{F}(\mathbf{x},\mathbf{y}) \end{pmatrix}}_{\boldsymbol{\chi}} \overset{Splitting}{\Longrightarrow} \underbrace{\begin{pmatrix} \dot{\mathbf{x}} \\ \dot{\mathbf{y}} \end{pmatrix} = \begin{pmatrix} \mathbf{G}(\mathbf{x},\mathbf{y}) \\ \mathbf{0} \end{pmatrix}}_{\boldsymbol{\chi}_1}; \qquad \underbrace{\begin{pmatrix} \dot{\mathbf{x}} \\ \dot{\mathbf{y}} \end{pmatrix} = \begin{pmatrix} \mathbf{0} \\ \mathbf{F}(\mathbf{x},\mathbf{y}) \end{pmatrix}}_{\boldsymbol{\chi}_2}. \tag{3}$$

For time stepping the split equations, a first order, one pass algorithm $\boldsymbol{\chi}_{2,\Delta t} \circ \boldsymbol{\chi}_{1,\Delta t}$ used here involves finding the algebraic variables $\mathbf{x}$ that satisfy the algebraic constraint with $\mathbf{y}$ fixed, followed by evolving the ODE variables $\mathbf{y}$ over $\Delta t = t_{n+1} - t_n$ with $\mathbf{x}$ fixed. In practice, the ODE variables are time integrated using a globally first order scheme, say e.g., Backward Euler. This algorithm constitutes a typical splitting step. The monolithic and split schemes are both selectively used in the hybrid scheme.

Remark 1
In addition to the one-pass algorithm $\boldsymbol{\chi}_{2,\Delta t} \circ \boldsymbol{\chi}_{1,\Delta t}$, one can reverse the orders by evolving the ODE variables first followed by updating the algebraic variables to obtain the alternate one-pass algorithm $\boldsymbol{\chi}_{1,\Delta t} \circ \boldsymbol{\chi}_{2,\Delta t}$. Both one pass algorithms when applied to index-1 DAEs are globally first order accurate. While analogous results are well known for pure systems of ODEs, they have been proved only recently [38] for index-1 DAEs. Furthermore, it is shown in [38] that the symmetric two-pass splits, $\boldsymbol{\chi}_{2,\Delta t/2} \circ \boldsymbol{\chi}_{1,\Delta t/2} \circ \boldsymbol{\chi}_{2,\Delta t/2}$ and $\boldsymbol{\chi}_{2,\Delta t/2} \circ \boldsymbol{\chi}_{1,\Delta t/2} \circ \boldsymbol{\chi}_{2,\Delta t/2}$ are also globally first order accurate when applied to DAEs. This result is contrary to global second order accuracy of two-pass splits for pure ODEs showing that an extra pass in the DAE context does not translate to an increase in global order of accuracy. Consequently, attention here is restricted to one-pass algorithms.

2.2. Hybrid Scheme and Error Control

The overall framework for a hybrid time stepping strategy is summarized in a flowchart in Fig. 1. As shown in the flow chart, the goal is to compute the solution numerically at time t_{n+1} in an efficient and accurate manner, given the solution at time t_n. For achieving this, the hybrid framework provides a choice between monolithic and split options for the current timestep, $[t_n, t_{n+1}]$. The algorithm begins by predicting stepsizes Δt_{split} and Δt_{mono}, assuming

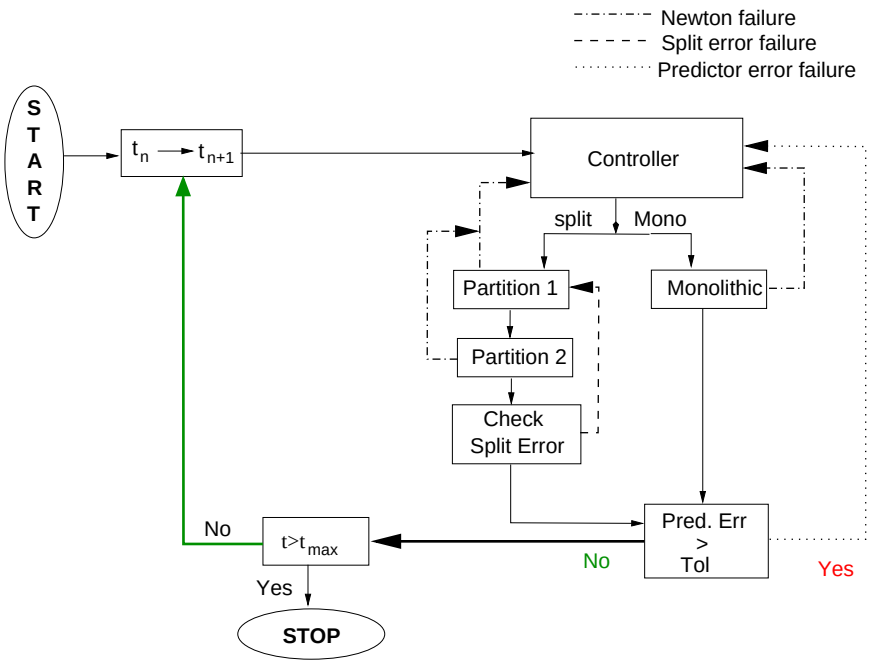

Figure 1. Flow chart for the adaptive hybrid time stepping

a split or a monolithic choice for the current timestep. Based on these stepsizes, the cost per unit stepsize is calculated for each choice. The splitting scheme or the monolithic scheme is chosen depending on which one delivers the smallest cost per unit stepsize. This choice guarantees efficiency. Once the solution at t_{n+1} is found, an a posteriori error check is made to satisfy a predictor error tolerance. If the choice for the current step is a splitting scheme, a splitting error tolerance is additionally checked. These error checks ensure accuracy and are central to the framework of the hybrid scheme.

2.3. Error Control

Predictor Error

Using the notation, where $\mathbf{z} = [\mathbf{x}, \mathbf{y}]^T$, the predictor error PE is given by

$$\begin{aligned} \text{PE} &= \mathbf{z}_{n+1} - \mathbf{v}_{n+1} && \text{(4a)} \\ &= \mathbf{z}[n+1, n, n-1](\Delta t^p)(\Delta t^p + \Delta t_1). && \text{(4b)} \end{aligned}$$

The difference term in Eqn. (4a) measures how fast the discrete solution is changing [26]. Therefore, the larger this difference, the larger would be the error associated with a time step to be controlled. As shown in Fig. 2, $\mathbf{v}_{n+1}$ denotes the linear extrapolation of the solution at times, t_n and t_{n-1}. Eqn. (4b) is obtained from a standard result on errors from polynomial

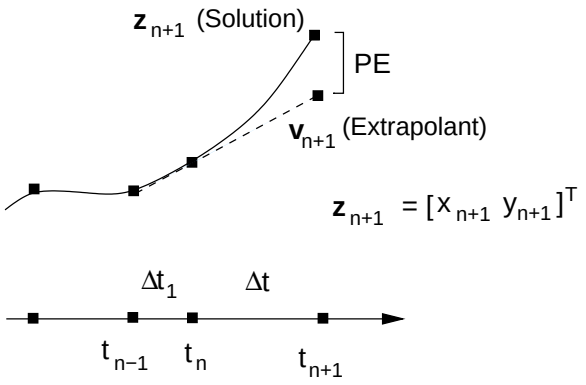

Figure 2. Schematic diagram explaining the Predictor Error.

extrapolation [32], where $\mathbf{z}[n+1, n, n-1]$ denotes the second divided difference[‡] computed from the solution at t_{n+1}, t_n and t_{n-1}. Further, $\Delta t^p = t_{n+1} - t_n$ is the current unknown stepsize, while $\Delta t_1 = t_n - t_{n-1}$ is the previous stepsize. Since, in Eqn. (4b), the predictor error depends on the unknown solution $\mathbf{z}_{n+1}$, it can only be used for an a posteriori error check. For predicting stepsize Δt^p, an a priori estimate for the predictor error is needed. We adopt the approximation

$$\text{Est. PE} = \mathbf{z}[n, n-1, n-2](\Delta t^p)(\Delta t^p + \Delta t_1), \tag{5}$$

where only the known solutions at previous time steps are utilized.

The stepsize Δt^p is obtained by setting $\|PE\|_a = tol$, where tol is a tolerance; this gives the following polynomial relation:

$$(\Delta t^p)(\Delta t^p + \Delta t_1) = \frac{tol}{\|\mathbf{x}[n, n-1, n-2]\|_a + \|\mathbf{y}[n, n-1, n-2]\|_a}. \tag{6}$$

Here, $\|\cdot\|_a$ denotes a discrete relative norm defined as:

$$\|(\cdot)\|_a = \sqrt{\sum_i \left(\frac{(\cdot)^i w_i}{rtol_{(\cdot)} \, |(\cdot)^i| + atol_{(\cdot)}} \right)^2}, \tag{7}$$

where $atol_{(\cdot)}$ and $rtol_{(\cdot)}$ are specified absolute and relative tolerances, respectively, and w_i is a weighting factor with integers i denoting components of vectors. The tolerances $atol_{(\cdot)}$ and $rtol_{(\cdot)}$ are typically selected to be different for the different field variables. Finally, once the solution $\mathbf{z}_{n+1}$ is found for the time step $[t_n, t_{n+1}]$, Eqn. (4b) is used to perform an a posteriori check for satisfying the tolerance tol. If the a posteriori check is successful and the current time step is a monolithic step, we save the current Δt^p in a history variable Δt^{prev}_{mono} for later use in

[‡]In general, the divided differences are defined recursively as: $\mathbf{z}[n+1, n, n-1, \ldots, n-i-1] = (\mathbf{z}[n+1, n, n-1, \ldots, n-i] - \mathbf{z}[n, n-1, \ldots, n-i-1])/t_{n+1} - t_{n-i-1}$, where the zeroth divided difference is defined as $\mathbf{z}[n+1] = \mathbf{z}_{n+1}$

decision making. On the other hand, if the a posteriori check fails, the stepsize is reduced and the time step is repeated.

The key advantage of using the predictor error as an error measure is that it doesn't distinguish whether the time discrete solution at previous time instants were obtained from a split or a monolithic choice. In other words, the algorithm for time integration is independent of error control. Consequently, predictor errors can be used for the adaptive time stepping of either a purely monolithic scheme or a hybrid time stepping scheme. The error formulation has the property that a smaller stepsize implies a smaller predictor error and vice versa. Therefore, tightening the predictor error tolerance implies convergence to the exact solution. The development of the predictor error measure is novel and is a key step in the formulation of the adaptive hybrid scheme. Commonly used error measures based on a truncation error (see references [18], [7]) simply do not separate the time stepping algorithm from error control.

Splitting Error

When an operator split choice is made for a particular time step, splitting errors have to be controlled in addition to the predictor errors. The splitting error in the discrete setting is defined as the difference between a monolithic solution and the split solution for the current time step, *i.e.*,

$$\text{Split Error (SE)} = \|\mathbf{z}^M_{n+1} - \mathbf{z}^s_{n+1}\|_a. \tag{8}$$

While the split solution $\mathbf{z}^s_{n+1}$ is known for the time step of interest, the monolithic solution $\mathbf{z}^M_{n+1}$ is unknown. However, the norm of the difference in Eqn. (8) can be computed in the following way. Assuming a first order method such as backward Euler to time integrate Eqn. (1), the monolithic residual evaluated on the split solution is

$$\mathbf{R}(\mathbf{z}^s_{n+1}) = \mathbf{R}(\mathbf{x}^s_{n+1}, \mathbf{y}^s_{n+1}) = \begin{pmatrix} \mathbf{G}(\mathbf{x}^s_{n+1}, \mathbf{y}^s_{n+1}) \\ \mathbf{y}^s_{n+1} - \mathbf{y}^s_n - \Delta t \mathbf{F}(\mathbf{x}^s_{n+1}, \mathbf{y}^s_{n+1}) \end{pmatrix}. \tag{9}$$

Using the monolithic residual $\mathbf{R}$ evaluated at the split solution, a single iterative update is performed. For example, if a Newton update is performed on $\mathbf{z}^s$,

$$\mathbf{z}^M_{n+1} - \mathbf{z}^s_{n+1} = -(\mathbf{D}_Z \mathbf{R} \mid_{\mathbf{z}^s_{n+1}})^{-1} \mathbf{R}(\mathbf{z}^s_{n+1}). \tag{10}$$

Since errors reduce asymptotically quadratically using the Newton scheme when $\mathbf{z}^s_{n+1}$ is close to the monolithic solution $\mathbf{z}^M_{n+1}$ (which satisfies the monolithic residual in (9), exactly), the ODE variables in $\mathbf{z}^s_{n+1}$ are $O([\Delta t^p]^2)$ and the algebraic variables are $O((\Delta t^p))$ approximations of their monolithic counterparts. Consequently, using a single Newton update, with asymptotic quadratic convergence, $\mathbf{z}^s_{n+1}$ is an $O([\Delta t^p]^2)$ approximation in the algebraic variables, and an $O([\Delta t^p]^4)$ approximation in the ODE variables to $\mathbf{z}^M_{n+1}$. Similar conclusions can be drawn when other iterative updates like Broyden [32] or Krylov updates [9] are made. We now compute an estimate of how much larger of a time step we could have taken, $\Delta t_{splitmax}$, via the relation below. If the split error satisfies a tolerance SE_{tol},

$$\frac{\Delta t_{splitmax}}{\Delta t^p} = \left(\frac{SE_{tol}}{SE}\right)^{1/m}, \tag{11}$$

where m (such that $1 < m \leq 2$) depends on the type of iterative update (*e.g.*, Krylov or Broyden or Newton). For a successful split step, we also save the current Δt^p in a history

variable Δt^{prev}_{split} for later use in decision making. If the a posteriori check fails to satisfy SE_{tol}, the step size is reduced according to Eqn. (11) and the timestep is repeated.

In summary, a predictor error measure that fundamentally separates the time integration algorithm from the error measure, and a scheme for computing the splitting errors in the context of general nonlinear operators makes an error based hybrid scheme a reality.

The full algorithmic details for the hybrid scheme control logic are enumerated as follows:

1. Compute the cost for monolithic and split options using stored history. The procedure for cost computation is summarized as follows:

   - Retrieve Δt^{prev}_{mono}, Δt^{prev}_{split} and $\Delta t_{splitmax}$, the latest successful monolithic and split stepsizes and a maximum possible split stepsize from a database.
   - Calculate Monocost = Cost/iteration $\times$ # of iterations for last successful stepsize, Δt^{prev}_{mono}.
   - Calculate Splitcost = $\sum_{partitions}$ Cost/iteration of Partition $\times$ # of iterations for partition with last successful stepsize, Δt^{prev}_{split}.

2. Calculate Δt_{mono} and Δt_{split}, the stepsizes for monolithic and split choices, for the next timestep $[t_n,\ t_{n+1}]$.

   - Compute Δt^p, the trial stepsize based on the estimated predictor error.
   - $\Delta t_{mono} = \min[5\Delta t^{prev}_{mono},\ \Delta t^p]$
   - Retrieve $\Delta t_{splitmax}$ from the history.
   - $\Delta t_{split} = \min[5\Delta t^{prev}_{split},\ \Delta t^p,\ \Delta t_{splitmax}]$.

3. **Decide** based on cost per unit stepsize, *i.e.*,
   IF $(\frac{\text{Monocost}}{\Delta t_{mono}} > \frac{\text{Splitcost}}{\Delta t_{split}})$
   Choose Split option
   ELSE
   Choose Monolithic Option
   END

   This scheme for choosing the best strategy and the best stepsize for the particular strategy leads to both efficiency and accuracy.
4. For every successful step, history information on the number of iterations of the iterative schemes is stored irrespective of whether the choice is monolithic or split. In order to keep the history as current as possible, either a split or a monolithic choice is never allowed consecutively more than N_{con} times.
5. When a split algorithm is chosen, iterations may fail to converge in either phase of the split within the limit, MAXITER . The reader is reminded that nonlinear algebraic equations have to be solved iteratively while updating the algebraic variables. Similarly, nonlinear algebraic equations may have to be solved for time integrating the ODEs whenever an implicit time integrator (e.g., Backward Euler) is utilized. In these cases, the stepsize is reduced by half and a split step is tried again. Similarly, when iterations fail during a monolithic step within the limit MAXITER, the stepsize is reduced and the monolithic step is repeated. This detects slow convergence or divergence of iterations and leads to robustness. Finally, only MAXTRY number of stepsize reductions are allowed

either in the splitting phases or the monolithic step failing which the time integration is terminated.

In summary, the error measures ensure accuracy while a cost based choice between monolithic and splitting options for each time step guarantees efficiency. Additionally, stepsize reductions to handle extreme nonlinearities ensure that iterative schemes converge leading to robustness. This completes the section on the hybrid scheme–the primary development in this paper.

3. Application of the Hybrid Scheme to a Diffusion-Deformation-Reaction Problem

As mentioned in the introduction, the motivation for developing a sophisticated hybrid time stepping scheme comes from the need to simulate silylation, a process step in microlithography[12]. The governing equations for silylation include global mass balance for solvent diffusion and mixture stress equilibrium for polymer deformation. The balance laws are derived in a finite deformation setting to accommodate large strains due to swelling and are only summarized here. Complete details can be found in Refs. [39, 16]. However, it is useful to mention that the coupling between solvent concentration M and polymer displacements $\mathbf{u}$ in the governing equations arises from the following: (1) a finite strain viscoelastic stress law for the polymer overstress in the deviatoric and pressure components with relaxation time, τ, dependent on M, (2) a solvent swelling pressure p_s dependent on M, (3) a jacobian determinant J dependent chemical potential μ in the solvent flux law and (4) a mobility coefficient B dependent on the solvent concentration and concentration R of reacted sites. The functional forms that define the various constitutive relations and therefore coupling terms introduce extreme nonlinearities and also introduce the physically consistent strong coupling.

3.1. Balance Laws

- *Solvent Mass Balance*

$$\dot{M} = \mathrm{DIV}[B(M,J,R)M\mathbf{C}^{-1}\mathrm{GRAD}\mu]. \tag{12}$$

Here, DIV and GRAD denote the divergence and the gradient operators in the coordinates X_A, $A = 1, 2, 3$ that define the reference placement of the dry polymer. Further, $\mathbf{C} = \mathbf{F}^T\mathbf{F}$ denotes the Right Cauchy-Green strain tensor, $\mathbf{F} : F_{iA} = \partial x_i/\partial X_A$ denotes the deformation gradient while R denotes the concentration of the reacted sites in the reference configuration. The spatial coordinates x_i, $i = 1, 2, 3$ define the deformed solvent-polymer mixture. The symbol $\dot{(\ )}$ denotes the material time derivative.

- *Stress Equilibrium (Quasi-static Case)*

$$\mathrm{DIV}[\mathbf{FS}] = \mathbf{0}. \tag{13}$$

Here, $\mathbf{S}$ denotes the 2^{nd} Piola-Kirchhoff stress tensor and inertial effects are ignored.

3.2. Constitutive Relations

- *Total Stress*

$$\mathbf{S} = Jp\mathbf{C}^{-1} + \mathbf{S}_{DEV}. \tag{14}$$

The stress $\mathbf{S}_{DEV}$ denotes a deviatoric component of $\mathbf{S}$ while p is the total pressure.

- *Deviatoric Stress*

$$\mathbf{S}^{\infty}_{DEV} = 2\rho_0 \frac{\partial \tilde{\psi}^E}{\partial \mathbf{C}} = 2\rho_0 J^{-\frac{2}{3}} \mathrm{DEV} \frac{\partial \tilde{\psi}^E}{\partial \tilde{\mathbf{C}}} \tag{15}$$

Here, $\mathbf{S}^{\infty}_{DEV}$ is a purely elastic contribution to the deviatoric stress, $\tilde{\mathbf{C}} = J^{-\frac{2}{3}}\mathbf{C}$ and $\mathrm{DEV}(\cdot) = (\cdot) - \mathrm{tr}((\cdot)^T\mathbf{C})\mathbf{C}^{-1}/3$ is the pull-back of the standard deviatoric operator to reference coordinates. In the simulations, the strain energy $\tilde{\psi}^E$ is provided by a modified Neo-Hookean model, i.e., $\tilde{\psi}^E = \mu^E(\mathrm{tr}\tilde{\mathbf{C}} - 3)$, where μ^E is the long term shear modulus. The total deviatoric stress, including a viscous contribution $\mathbf{Q}$ is given by

$$\mathbf{S}_{DEV} = \mathbf{S}^{\infty}_{DEV} + 2\rho_0 J^{-\frac{2}{3}} \mathrm{DEV}[\mathbf{Q}]. \tag{16}$$

- *Total Pressure*

$$p = p^{\infty} + p_s + q. \tag{17}$$

The total pressure has an elastic contribution p^{∞} and a viscoelastic overstress contribution q from the polymer skeleton while p_s denotes the solvent pressure.

$$p^{\infty} = c_b[c_2 J + c_4 - (c_2 - 1)^2/(c_2 J + c_4)], \tag{18a}$$

$$p_s = \rho_0 c_s \ln\left[\frac{c_1(c_2 J + c_4)}{c_2 J + c_4 - c_5 M}\right]. \tag{18b}$$

In these expressions, c_s, c_b and c_i, $i = 1, \ldots, 5$ are material constants.

- *Viscoelastic over-stress*

$$\dot{q} + \frac{q}{\tau(M, J)} = \beta \dot{p}^{\infty}, \tag{19}$$

$$\dot{\mathbf{Q}} + \frac{\mathbf{Q}}{\tau(M, J)} = \alpha \overline{\left[\frac{\partial \tilde{\psi}^E}{\partial \tilde{\mathbf{C}}}\right]}^{\cdot}. \tag{20}$$

In these evolution equations for the viscoelastic overstress, the relaxation time τ is concentration and deformation dependent. Further, α and β are material constants.

- *Chemical Potential*

$$\mu = \rho_0[\ln(c_1 c_5 M) - \ln(c_2 J + c_4 - c_5 M)]. \tag{21}$$

- *Reaction Evolution*

$$\dot{R} = K_r \frac{(R_{max} - R)M}{J}. \tag{22}$$

In the evolution law for reacted sites concentration R, R_{max} denotes the maximum concentration of sites at each point in the polymer available for reaction with the solvent and K_r is the reaction constant. No separate balance law for the reacted sites is assumed. The

Table I. Choice of functions for diffusion coefficient, the relaxation time, and the current free volume

	Functional Form	Parameters
Diffusion Mobility B	$B(M,\, J,\, R) = B_0(1 + \xi(M/J)^2 + \chi R^2)$	$B_0,\, \xi,\, \chi$
Relaxation Time τ	$\tau(M,\, J)) \;= \tau_0 g(M,\, J)$	τ_0
Relaxation Time Function g	$g(M,\, J) = \exp(B_d(f - f_0)/(f_0 f))$	$B_d,\, f_0$
Current Free Volume f	$f(M,\, J) \;= f_0 + a_\eta M/J$	a_η

silylating agent is a mixture (90%-10% by weight) of a liquid solvent and a silicon containing reactant that reacts with the polymer. Assuming that the solvent acts as a perfect conduit for the silicon containing compound and that the silicon compound is always available for reaction until all the reaction sites R_{max} are consumed, the above evolution for the reaction process can be justified (see Ref. [39] for complete details).

Further, the functional forms and parameters for various coefficients are tabulated in Table. I.

3.3. Spatial Discretization of the Balance Laws

The hybrid scheme is applicable for the DAEs arising from spatial discretization of the balance laws. Spatial discretization of the balance laws is performed using standard C^0 finite elements (see e.g., [20]) for the spatial fields. For the mechanical problem, the displacement field $\mathbf{u}$ defined as $\mathbf{u} = \mathbf{x} - \mathbf{X}$ is interpolated linearly through shape functions N^I, $I = 1 \ldots, N_{nodes}$, in terms of a vector of nodal displacements $\mathbf{U}$. Therefore, $\mathbf{u} = \mathbf{N}\mathbf{U}$, where $\mathbf{N}$ is a matrix containing N^Is. For the diffusion problem, there are two choices for the interpolation fields. Either the concentration M or a mixed variable, activity $A = \exp(\mu)$ can be linearly interpolated in terms of their nodal values. When concentration Dirichlet boundary conditions are specified, the field M is the natural choice for interpolation. However, in this paper, a formulation in terms of activity A is utilized for reasons explained below.

3.4. Formulation in terms of Activity

The diffusion problem has two physically relevant boundary conditions: (1) exposure of the dry polymer to a solvent and (2) insulation to solvent diffusion. The physically correct boundary condition for exposure to the solvent is to specify an activity A (and not solvent concentration) on the polymer boundary [13, 16]. The second boundary condition corresponds to specifying the flux given in terms of the gradient of μ (or equivalently A). Motivated by the physically relevant boundary conditions which are in terms of activity and its gradient, the mass and momentum balance equations are written in terms of the activity and the deformation as the primary variables through the transformation:

$$A = \exp(\mu) = \frac{c_1 M}{c_2 J + c_4 - M}, \tag{23}$$

$$M = M(A, J) = \frac{(c_2 J + c_4) A}{c_1 + A}\,. \tag{24}$$

Such a formulation, with activity as a primary variable, avoids the following difficulties.

1. In the formulation where concentration M is the primary variable, boundary conditions in terms of activity have to be imposed as mixed boundary conditions. From, Eqn. (24), specifying activity implies imposing a mixed boundary condition which nonlinearly relates M and J. Implementing these boundary conditions in a finite element setting is rather inconvenient, if not impossible.
2. The gradient of the chemical potential takes the form

$$\frac{\partial \mu}{\partial \mathbf{x}} = \frac{\partial \mu}{\partial M}\frac{\partial M}{\partial \mathbf{x}} + \frac{\partial \mu}{\partial J}\frac{\partial J}{\partial \mathbf{x}}, \tag{25}$$

when displacements $\mathbf{u}$ and concentration M are used as primary variables. From Eqn. (25), the spatial derivatives $\partial J/\partial \mathbf{x}$ of the Jacobian determinant, or equivalently, second derivatives of $\mathbf{u}$ are required. This would lead to difficult continuity requirements on the finite element shape functions associated with solvent mass balance.

3.5. Matrix Forms

The Galerkin finite element method can be stated in terms of finding the C^0 fields, $\mathbf{u}$ and A (or equivalently, nodal vectors $\mathbf{U}$ and $\mathbf{A}$) satisfying the weak forms of solvent mass balance and mixture stress equilibrium.

The weak from of the solvent mass balance given by Eqn. (12) states: Find $A \in \mathcal{S}_{\mathcal{A}} = \{A \in H^1(\Omega); A = A_0 \text{ for } \mathbf{x} \in \Gamma_A\}$, $\forall$ variations δA such that,

$$\begin{aligned} G_A(A, \mathbf{u}; \delta A) = &\int_{\bar{\Omega}} \frac{dM(A,\, J)}{J dt}\, \delta A \, d\mathbf{x} \\ &+ \int_{\bar{\Omega}} B(M(A,\, J,\, R), J) \frac{M}{AJ} \text{grad} A \cdot \text{grad} \delta A \, d\mathbf{x} - \int_{\bar{\Gamma}_h} \breve{\mathbf{h}} \cdot \mathbf{n} \, d\mathbf{x} = \mathbf{0}. \end{aligned} \tag{26}$$

In Eqn. (26), the integrals have been transformed in terms of spatial coordinates $\mathbf{x}$ using solvent mass balance (12). Further, $\breve{\mathbf{h}}$ is the specified flux on the boundary of $\phi(\Omega)$, the deformed body, with $\mathbf{n}$ being its outward normal.

The weak form for the mixture stress equilibrium states: Find $\mathbf{u} \in \mathcal{S}_{\mathbf{u}} = \{u_i \in H^1(\Omega),\ i = 1, 2, 3; \mathbf{u} = \mathbf{u}_0 \text{ for } \mathbf{x} \in \Gamma_{\mathbf{u}}\}$, $\forall$ variations $\boldsymbol{\delta}\mathbf{u}$ such that,

$$H_{\mathbf{u}}(A, \mathbf{u}; \boldsymbol{\delta}\mathbf{u}) = \int_{\bar{\Omega}} [p\mathbf{I} + \text{dev}\, \boldsymbol{\sigma}(A,\, J)] \cdot \text{grad}(\boldsymbol{\delta}\mathbf{u})\, d\mathbf{x} - \int_{\bar{\Gamma}_{\mathbf{t}}} \breve{\mathbf{t}} \cdot \boldsymbol{\delta}\mathbf{u} = \mathbf{0}. \tag{27}$$

In Eqn. (27), $\text{dev}(\cdot) = (\cdot) - \text{tr}(\cdot)\,\mathbf{I}/3$ is the deviatoric projection operator. The Cauchy stress tensor $\boldsymbol{\sigma}$ is the push forward of the Second Piola stress $\mathbf{S}$, and p is the pressure. Here, $\breve{\mathbf{t}}$ is the specified traction on the deformed boundary.

Since, the weak forms (26) and (27) hold for all admissible variations δA and $\delta \mathbf{u}$, one can write the following DAEs indicated in terms of their functional dependencies.

$$\text{Mass Balance:} \quad \frac{d\mathbf{M}(\mathbf{A}, \mathbf{U})}{dt} + \mathbf{R}(\mathbf{A}, \mathbf{U}; R) = \mathbf{f}, \tag{28a}$$

$$\text{Momentum Balance:} \quad \mathbf{S}(\mathbf{A}, \mathbf{U}; \mathbf{Q}, q) - \mathbf{s} = \mathbf{0}, \tag{28b}$$

where

$$\mathbf{M}(\mathbf{A},\mathbf{U}) = \mathop{\mathsf{A}}_{e=1}^{n_{el}} \mathbf{m}^{(e)}_{[N_{en}\times 1]}: \quad \mathbf{m}^{(e)}_{(I,1)} = \int_{\mathbf{\Omega}_e} N^I \frac{M(\mathbf{A},\mathbf{U})}{J} d\mathbf{x}, \tag{29}$$

$$\mathbf{R}(\mathbf{A},\mathbf{U};R) = \mathop{\mathsf{A}}_{e=1}^{n_{el}} \mathbf{r}^{(e)}_{[N_{en}\times 1]}: \quad \mathbf{r}^{(e)}_{(I,1)} = \int_{\mathbf{\Omega}_e} B(\mathbf{A},\mathbf{U};R) \frac{M(\mathbf{A},\mathbf{U})}{A} \mathrm{grad}N^I.\mathrm{grad}A \, d\mathbf{x}, \tag{30}$$

$$\mathbf{S}(\mathbf{A},\mathbf{U};\mathbf{Q},q) = \mathop{\mathsf{A}}_{e=1}^{n_{el}} \mathbf{s}^{(e)}_{[(N_{en}.ndm)\times 1]}:$$

$$\mathbf{s}^{(e)}_{([I-1]\times ndm+K,1)} = \int_{\mathbf{\Omega}_e} \sum_{k=1}^{ndm} \frac{\partial N^I}{\partial x^k} [\mathrm{dev}\boldsymbol{\sigma}(\mathbf{U},\mathbf{A},\mathbf{Q}) + p(\mathbf{U},\mathbf{A},q)\mathbf{I}]_{Kk} \, d\mathbf{x}. \tag{31}$$

Here, $\mathbf{U}$ and $\mathbf{A}$ denote the vector of nodal displacements and nodal activities. Further, N_{en} denotes the number of nodes in the element, n_{el} denotes the number of elements, and ndm, the dimension of the problem. The fields, A and J are calculated for each element in terms of nodal values. The various integrals are computed numerically using Gaussian quadrature. Since numerical quadrature is used, the viscoelastic stresses $\mathbf{Q}$ and q, and the reacted sites R are evolved only at each of the quadrature points in an element. Numerical time integration is used for their evolution as well.

The solvent mass balance equations in (28a) constitute a system of ordinary differential equations. The stress equilibrium equations in (28b) result in algebraic constraints. Since, the derivative $d\mathbf{S}(\mathbf{A},\mathbf{U};\mathbf{Q},q)/d\mathbf{U}$ is assumed to be invertible, the set of equations in (28a) and (28b) constitute a system of Index-1 DAEs. The invertibility assumption is equivalent to assuming that no bifurcation phenomena in the stress equilibrium problem is witnessed during the time integration of the DAEs. In the silylation examples, this assumption was always found to be satisfied.

4. Implementation Details

Based on the canonical form for the DAEs considered, solvent concentration M and polymer displacements $\mathbf{u}$ are the respective ODE and DAE variables for time splitting. However, due to the reasons stated in the previous section, the activity field A is interpolated at the nodes, making the nodal vectors $\mathbf{A}$ and $\mathbf{U}$ as the primary unknowns. Due to the involvement of activity nodal variables which is unusual, further implementation details are provided here. Consistent with the theory presented earlier, the splitting step is still effected by fixing solvent concentration at element quadrature points in the deformation phase although activity is the nodal variable. Before providing the details of a typical splitting step, a typical monolithic step is summarized.

4.1. Implementation of the Monolithic Algorithm

The monolithic scheme for time stepping from t_n to t_{n+1} can be summarized as solving for nodal values $\mathbf{A}_{n+1}$ and $\mathbf{U}_{n+1}$ given their values at t_n. Using a backward Euler discretization,

the following system of equations is obtained.

Mass Balance:

$$\frac{\mathbf{M}(\mathbf{A}_{n+1},\mathbf{U}_{n+1})-\mathbf{M}(\mathbf{A}_n,\mathbf{U}_n)}{\Delta t}+\mathbf{R}(\mathbf{A}_{n+1},\mathbf{U}_{n+1};R^{(i)}_{n+1})=\mathbf{f}_{n+1}, \tag{32a}$$

Momentum Balance:

$$\mathbf{S}(\mathbf{A}_{n+1},\mathbf{U}_{n+1},\mathbf{q}_{n+1})-\mathbf{s}_{n+1}=\mathbf{0}, \tag{32b}$$

Viscoelastic Evolution:

$$\frac{q^{(i)}_{n+1}-q^{(i)}_n}{\Delta t}+\frac{q^{(i)}_{n+1}}{\tau(M_{n+1},\,J_{n+1})}=\beta\frac{p^\infty\mid_{t_{n+1}}-p^\infty\mid_{t_n}}{\Delta t}, \tag{33a}$$

$$\frac{\mathbf{Q}^{(i)}_{n+1}-\mathbf{Q}^{(i)}_n}{\Delta t}+\frac{\mathbf{Q}^{(i)}_{n+1}}{\tau(M_{n+1},\,J_{n+1})}=\alpha\frac{\frac{\partial\tilde{\psi}^E}{\partial\tilde{\mathbf{C}}}\mid_{t_{n+1}}-\frac{\partial\tilde{\psi}^E}{\partial\tilde{\mathbf{C}}}\mid_{t_n}}{\Delta t}, \tag{33b}$$

Reaction Evolution:

$$\frac{R^{(i)}_{n+1}-R^{(i)}_n}{\Delta t}=K_r\frac{(1-R^{(i)}_{n+1})M(A_{n+1},J_{n+1})}{J_{n+1}}. \tag{33c}$$

In these equations, the unknown nodal activities and displacements form the driving variables. In Eqns. (33a), (33b) and (33c), the index i runs from 1 to the number of quadrature points N_{quad}. A monolithic step in the hybrid scheme involves evolving both the nodal displacements and activities simultaneously by solving the complete system of nonlinear algebraic equations (32a)–(33c) at each time step. In the next section, the details of a typical split step are discussed.

4.2. Implementation of the Splitting Algorithm

Deformation Phase: ($\dot{\mathbf{M}}=\mathbf{0}$)

1. Given nodal values $\mathbf{U}_n$ and $\mathbf{A}_n$ at time t_n, the concentration field M_n is calculated within each element from Eqn. (24). Here, the nodal values $\mathbf{U}_n$ and $\mathbf{A}_n$ are linearly interpolated in a C^0 manner. However, the Jacobian determinant J is only piecewise continuous, so is M_n (see Fig. 3 for a depiction in the 1-D case).
2. The unknown $\mathbf{U}_{n+1}$ is solved from mixture stress equilibrium (32b) by holding M_n fixed pointwise in the interior of each element. In particular, M_n is held fixed at each quadrature point while calculating the contribution from swelling pressure p^s and viscoelastic stresses q and $\mathbf{Q}$. Fixing M_n is a special case of fixing the assembled global vector $\mathbf{M}_n$ (i.e., $\dot{\mathbf{M}}=\mathbf{0}$), a fact that is used in the accuracy analysis later.
3. The visco-elastic stresses are evolved in this phase, with a fixed M_n and reacted site concentration R_n.

A few remarks on the splitting implementation details can be made here.

Remark 2

In the deformation phase, nodal activities would still evolve due to displacement evolution even though the concentration is held fixed at the quadrature points. However, this intermediate nodal activity is never explicitly calculated. In the diffusion phase, using backward Euler

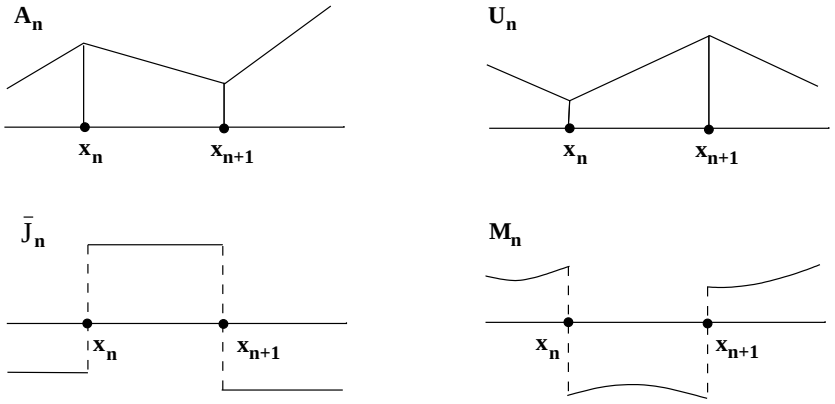

Figure 3. Illustration of the Splitting Algorithm in the 1-D case.

time integration, only nodal activities $\mathbf{A}_{n+1}$ at time t_{n+1}, and $\mathbf{A}_n$ at time t_n (for calculating $M_n = M_n(\mathbf{U}_n, \mathbf{A}_n)$) are actually needed.

Remark 3
The splitting scheme used here corresponds to the well-known "adiabatic splitting" algorithm [3] in the context of linear thermoelasticity. In that context, temperature plays an analogous role to activity while entropy corresponds to solvent concentration. Adiabatic splitting guarantees unconditional stability for the thermoelastic case by satisfying the contractivity of an energy norm. Even in the present context which is nonlinear, one can show that the free energy function decreases with time. However, the free energy need not induce a norm as in the linear thermoelastic context. This makes the splitting algorithm only dissipative in the free energy rather than being contractive in the energy norm of the solution (see [39] for a discussion). In spite of this, the adiabatic splitting is adopted here to ensure that the splitting algorithm is dissipative and consistent with the evolution of the time-continuous DAEs.

Remark 4
The norm adopted for calculating the predictor and splitting errors for the silylation problem is a mass-weighted norm. Accordingly, in Eqn. (7) w_i is computed as the lumped nodal mass for a unit density. This norm is the discrete analogue of the standard L_2 norm.

5. Numerical Examples

The numerical examples are provided here to illustrate the following: (1) strong coupling and extreme nonlinearities of the silylation problem, (2) successful application the hybrid scheme to simulate silylation resulting in an accurate solution with large savings in both 2- and 3-D situations.

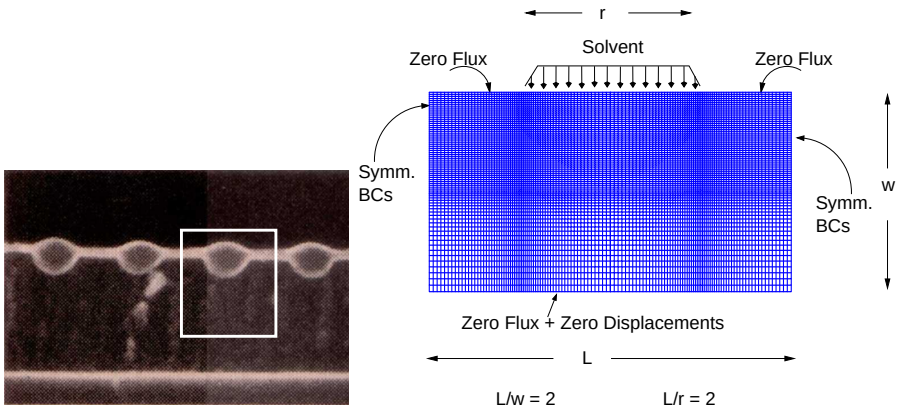

Figure 4. Left: SEM cross-section of a Silylated Photoresist [19]. Right: Geometry and Boundary Conditions of a Trench.

5.1. Silylation of a Trench in an array of lines

In this example, silylation of a single trench in an array of trenches, shown in Fig. 4, is simulated under 2-D plane strain conditions. The boundary conditions shown in Fig. 4 include symmetry boundary conditions on the lateral edges and zero solvent flux and zero displacements for the bottom. The top surface is free to expand and cross-linked regions are modeled by specifying zero flux. Solvent exposure to the uncrosslinked regions is specified through a unit solvent activity. The solvent is selectively diffused and reacted into the uncross-linked regions forming a protective cap which is resistant to subsequent etching as shown in Fig. 4. A finite element mesh with 4608 elements, 9216 displacement unknowns and 4709 activity unknowns is considered. Since, convergence of DAE solutions implies only convergence to the spatially discrete problem, a fine mesh such as the one chosen is needed to minimize errors in the spatial solution.

The material parameters for this simulation are listed in Table II. These parameters simulate a liquid phase silylation of a Shipley SPR505a polymer [4, 5] with the silylating agent consisting of a mixture of Xylene, a polymer solvent, and Hexamethylcyclotrisilazane(HMCTS), a reacting silicon compound. As experimentally observed, the polymer swells by 40% on silylation. The other key experimental features expected from the simulation include a sharp silylation front separating silylated and unsilylated regions, and silylation depths at the center-line varying linearly with time. The latter feature leads to a linear increase of cumulative reacted sites with time. This fact is experimentally verified by measuring energy absorbance of 1240–1280 cm^{-1} wavelength radiation by reaction bonds during a Fourier Transform Infrared (FTIR) Spectroscopic experiment [5]. The material parameters listed in Table II reflect a 3 orders of change in solvent mobility B during the simulation when the polymer changes from a dry to a fully swollen gel. Similarly, the polymer relaxation times τ decrease by 6 orders of magnitude to reflect a glass to rubber transition in the presence of the solvent. Further, the reaction constant K_r ensures a fast chemical reaction. These parameters replicate experiments but at the same time introduce extreme nonlinearities and a strong coupling.

For the numerical simulation, the IBVP is non-dimensionalized (see Appendix-A). For this non-dimensional form, the time stepping parameters and error controls chosen are listed in

μ	0.116 Mpa	$a_{\eta,p}$	0.3672 cm^3/gm	$a_{\eta,dev}$	0.3672 cm^3/gm
B_d	1/2.303	$\tau_{0,p}$	30s	$\tau_{0,dev}$	6s
α	1×10^3	β	5×10^2	c_b	1.71 $\times 10^2$
ξ	1.58×10^4 cm^6/gm^2	c_1	1.0	c_2	1.025
c_3	0.0	c_4	-1.0	c_5	0.51 cm^3/gm
B_0	7.79 $\times 10^{-6}$ μm^2/s	K_r	2.95 $\times 10^{-10}$ cm^3/gm.s	χ	10

Table II. Material Properties for the 2-D Silylation Example

Table III. Parameters for Adaptive Time Stepping

Δt_{min}	1×10^{-7}	a_{tol}	1×10^{-4}
r_{tol}	5×10^{-4}	MAXTRY	5
$\|SE\|_a^u$	5×10^{-5}	$\|SE\|_a^A$	4×10^{-5}
N_{con}	5	MAXITER	10

Table III. For cost comparison, two versions of the hybrid scheme are used. In the unsymmetric version, the stiffness matrix for the nodal displacements $\mathbf{U}$ used in the deformation phase is unsymmetric. In the symmetric version (see Appendix-B), an approximate viscoelastic contribution to the stress-equilibrium residual is used. This results in a symmetric stiffness matrix in the deformation phase. As a note, the full stiffness matrix of the coupled problem is always unsymmetric. Full Newton iterations were used as the problem is highly nonlinear[§]. The hybrid scheme which takes both monolithic and splitting steps during the simulation is compared with a purely monolithic scheme with the same error controls and time stepping parameters listed in Table III.

The evolution of normalized reaction fronts is plotted in Fig. 5 at 30, 60 and 90 sec. The first column corresponds to the monolithic calculation while the second and third correspond to the unsymmetric and symmetric versions of the hybrid scheme. From the plots, the reaction fronts from the 3 simulations with the specified tolerances match perfectly. For obtaining such high fidelity solutions, the cost statistics on a Pentium 3.1GHz 512MB RAM are compared at times $t = 30$, 60 and 120 sec of the simulation in Tables IV, V and VI. Based on CPU times, the symmetric hybrid scheme, for example, is about 2.17 times more efficient than the purely monolithic version at $t = 30$ sec. At $t = 60$ sec, the benefit ratio drops to 1.77 and further down to 1.47 at $t = 120$ sec for the symmetric hybrid scheme. This observation shows the necessity for a hybrid scheme. As the solvent diffuses and reacts deeper against greater swelling constraints, the coupling becomes stronger and splitting errors start dominating. Even though split time steps are favored in the hybrid scheme, the allowable stepsize to control splitting errors drops. In the current simulation, at $t = 60$ sec, the symmetric hybrid version, for example, takes

[§]Alternate inexpensive schemes like the modified Newton and Newton Krylov methods were attempted. However, they lead to severe convergence problems for the iterative solution of the nonlinear equations presented here.

Table IV. Cost Statistics for the 2-D silylation example at $t = 30$ sec, NM = # of successful Monolithic Steps, NS = # of Successful Split Steps up to t = 30sec

Scheme	Mono.	Split-1	Split-2
CPU time (sec)	2.6848e+04	1.4744e+04	1.2353e+04
ratio	2.17	1.19	1.0
Mono. iter.	5337	1638	1623
Mech. iter.	–	2892	2968
Conc. iter.	–	1837	1890
NM	571	175	163
NS	–	491	508
$\Delta t_{avg}(sec)$	5.25×10^{-2}	4.50×10^{-2}	3.89×10^{-2}

Table V. Cost Statistics for the 2-D silylation example, NM = # of successful Monolithic Steps, NS = # of Successful Split Steps up to t = 60sec

Scheme	Mono.	Split-1	Split-2
CPU time (sec)	8.3228e+04	6.0215e+04	4.7137e+04
ratio	1.77	1.28	1.0
Mono. iter.	16076	6278	5710
Mech. iter.	–	13230	13820
Conc. iter.	–	7106	7423
NM	1653	612	566
NS	–	2050	2176
$\Delta t_{avg}(sec)$	3.63×10^{-2}	2.25×10^{-2}	2.19×10^{-2}

Table VI. Cost Statistics for the 2-D silylation example, NM = # of successful Monolithic Steps, NS = # of Successful Split Steps up to t= 120sec

Scheme	Mono.	Split-1	Split-2
CPU time (sec)	2.0763e+05	1.7823e+05	1.4136e+05
ratio	1.47	1.26	1.00
Mono. iter.	41159	18794	17003
Mech. iter.	–	38851	42354
Conc. iter.	–	19949	21729
NM	4105	1828	1675
NS	–	5697	6421
$\Delta t_{avg}(sec)$	2.92×10^{-2}	1.59×10^{-2}	1.48×10^{-2}

21% monolithic and 79% splitting steps. There might be a situation where stepsizes based on splitting errors are so restrictive that it is more efficient to go fully monolithic. In a nonlinear problem, it is impossible to determine the coupling strength a priori and choose stepsizes accordingly to control splitting errors. This is the primary reason why splitting schemes with varying moderate/strong coupling have met with limited success. Meaning that for large stepsizes when they are efficient, they become inaccurate. Our hybrid scheme allows us to automatically avoid this problem.

The stepsize sequences for the entire simulation $t \in [0, 120]$ using the monolithic and the hybrid schemes are shown in Fig. 6. For all 3 simulations, stepsizes vary by 3 orders of magnitude making a strong case for stepsize adaptivity. Even though the solvent diffusion and polymer deformation appear monotonic, the stepsize variation is caused by large changes in mobility, swelling pressure and polymer relaxation times once the solvent front approaches a line of elements in the unsilylated region. Consequently, small stepsizes are needed both for Newton convergence as well as controlling predictor and split errors. Once the line of elements has swollen and the changes in mobility and relaxation times accommodated, the time stepping scheme gradually reverts to larger stepsizes. The cycle is repeated when the solvent front moves to a new line of elements leading to a near cyclic variation.

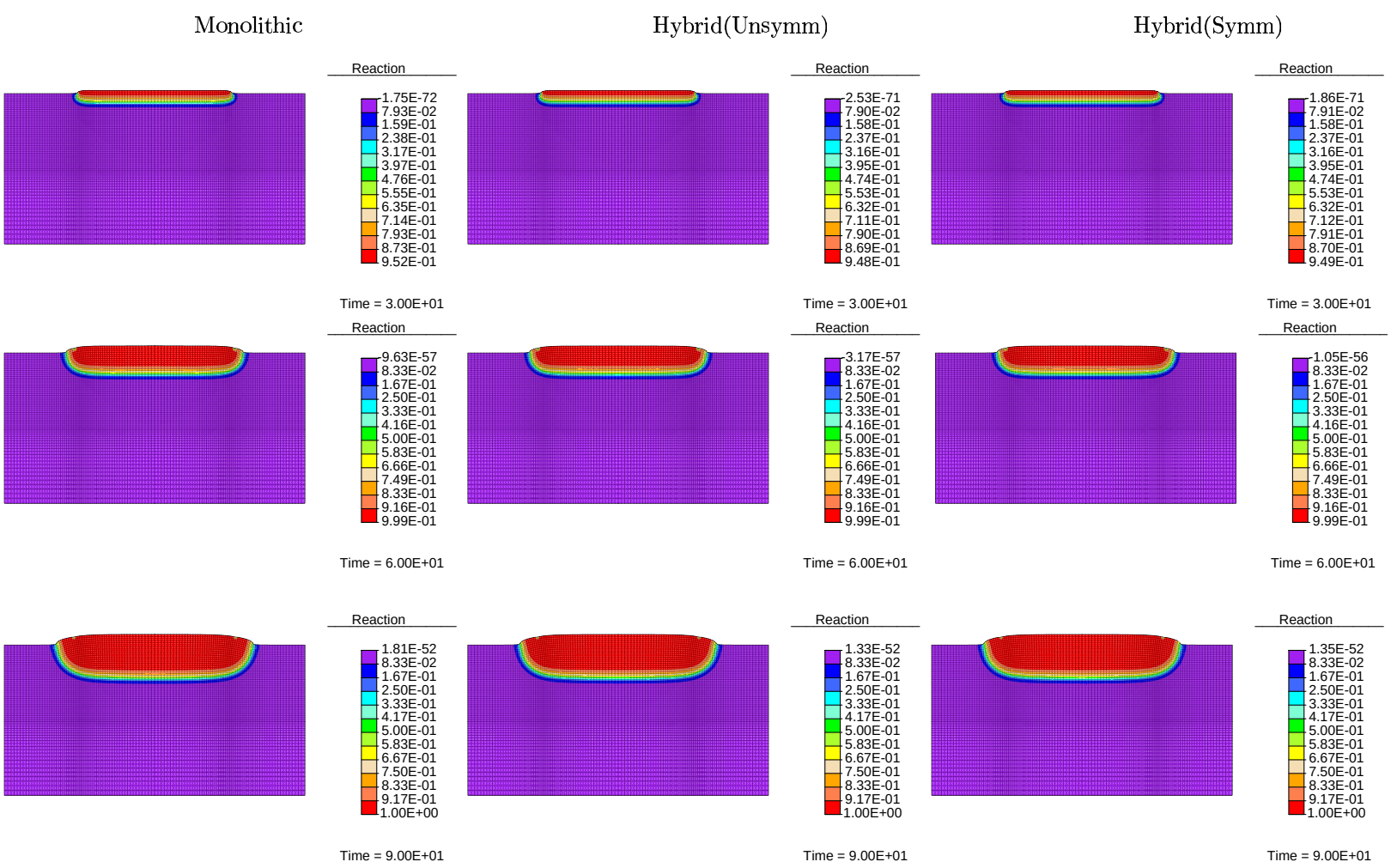

Figure 5. Evolution of Reaction Fronts for the silylation of the 2-D trench.

Table VII. Non-dimensional material properties for the 3-D examples

μ	8.32×10^{-3}	$a_{\eta,p}$	0.7	$a_{\eta,dev}$	0.7
B_d	0.43	$\bar{\tau}_{0,p}$	1.0	$\bar{\tau}_{0,dev}$	0.2
α	1×10^3	β	5×10^2	c_b	1.28×10^{-3}
ξ	6×10^4	c_1	1.0	c_2	1.025
c_3	0.0	c_4	-1.0	c_5	1.0

Table VIII. Parameters for Adaptive Time Stepping

Δt_{min}	1×10^{-7}	a_{tol}	5×10^{-5}
r_{tol}	2×10^{-4}	MAXTRY	5
$\|SE\|_a^u$	1×10^{-5}	$\|SE\|_a^A$	4×10^{-5}
N_{max}	5	MAXITER	10

5.2. Silylation of a 3-D L-shaped Pattern

As a 3-D application, silylation of L-shaped patterns shown in Fig. 7 is considered. One such pattern with geometry and boundary conditions is also shown in Fig. 7. This simulation is important for studying the effect of stresses on corner rounding and silylation depth. As before, the polymer slab is fixed at the bottom and impermeable to the solvent. As a good approximation, symmetry boundary conditions are assumed for the lateral surfaces. Excepting the L-shaped region where solvent exposure is modeled by specifying unit activity, the rest of the top surface is impermeable to model cross-linking. Further, zero tractions are prescribed for the top surface. Non-dimensional equations which are appropriate for understanding the qualitative behavior, are solved for this example. The reason being, experiments providing silylation depths versus time are unavailable for the 3-D L-pattern example.

The finite element mesh has 11094 solid 3-D elements, with 33792 displacement and 13137 activity unknowns. The dimensionless material parameters are listed in Table VII. The time stepping parameters and error controls for this different problem are listed in Table VIII. For this example, the unsymmetric hybrid version always favored monolithic steps¶. Therefore, the results from purely monolithic and the symmetric version of the hybrid scheme are presented. Fig. 8 shows the reaction fronts at non-dimensional time $\theta = 0.8$, the end of the simulation. As in the 2-D case, the reaction fronts remain sharp and match within 1% in their location from both the adaptive monolithic and the adaptive hybrid scheme. In Fig. 9, the slab is sliced along plane A (as shown in Fig. 8) and reaction contours are plotted on the undeformed polymer. It can be seen that stresses have a negligible influence on silylation depth. Further, the corners remain sharp, consistent with experiments which justify a stress-inhibited diffusion

¶In the 3-D case, the ratio of displacement to activity unknowns is roughly 3:1 as against 2:1 in the 2-D case. Consequently, the cost of unsymmetric solves in each phase of the split in the 3-D example supersedes the cost of monolithic unsymmetric solves.

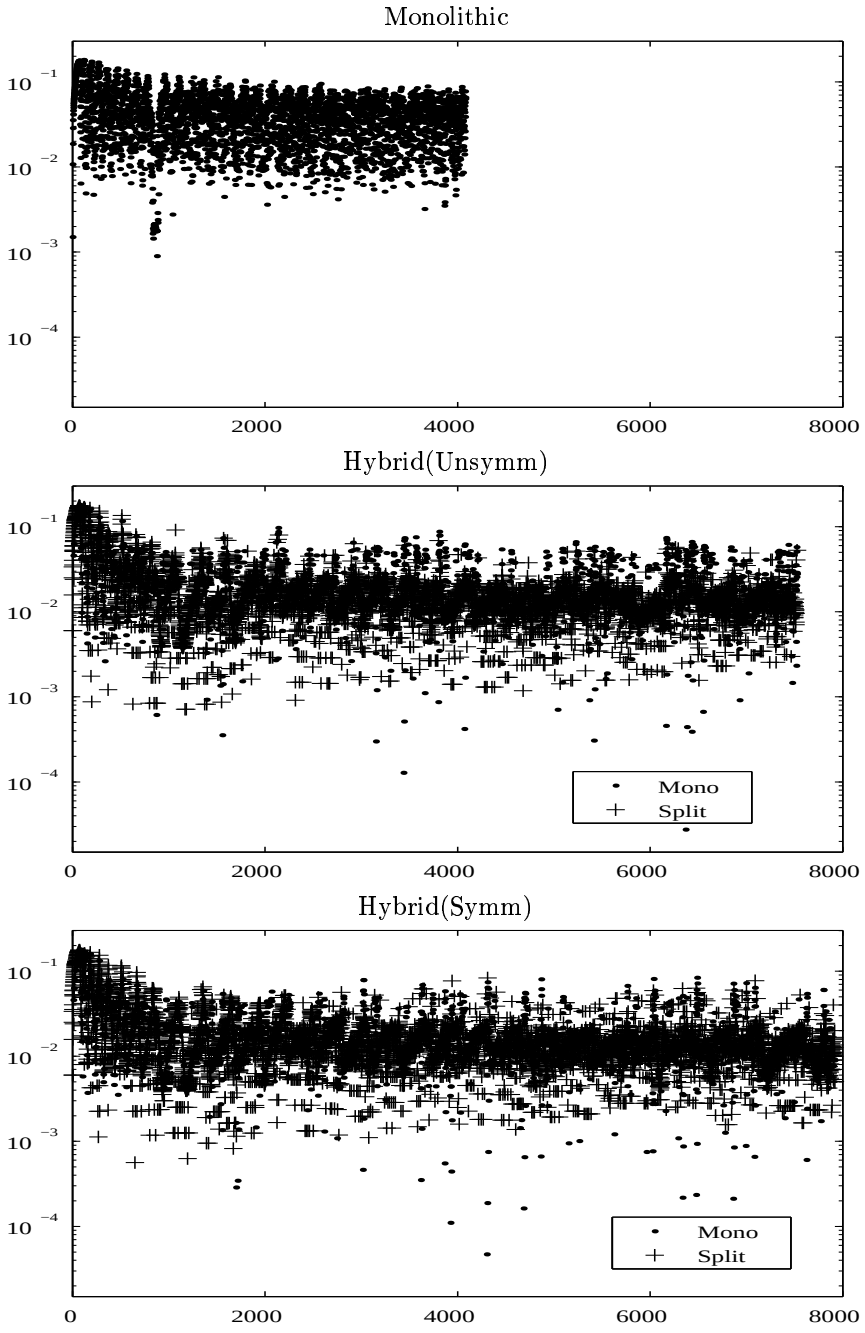

Figure 6. Stepsize Sequence for the silylation of the 2-D trench. X-axis: Step #, Y-axis: Log[Δt] in Sec.

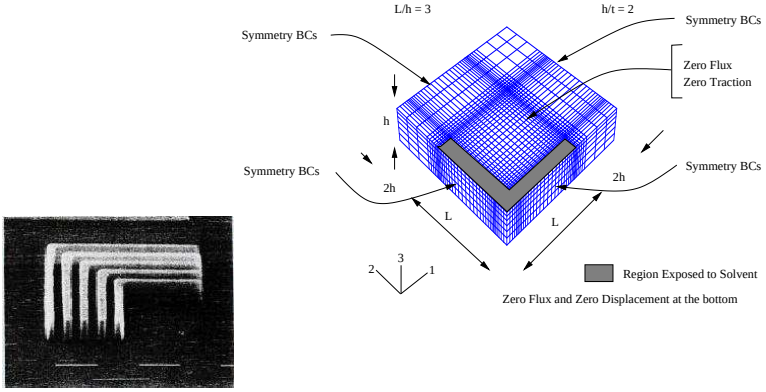

Figure 7. Left: SEM image of an etched photoresist [5]. Right: Geometry and Boundary Conditions of the L-pattern 3-D slab.

model where negative pressures prevent corner rounding.

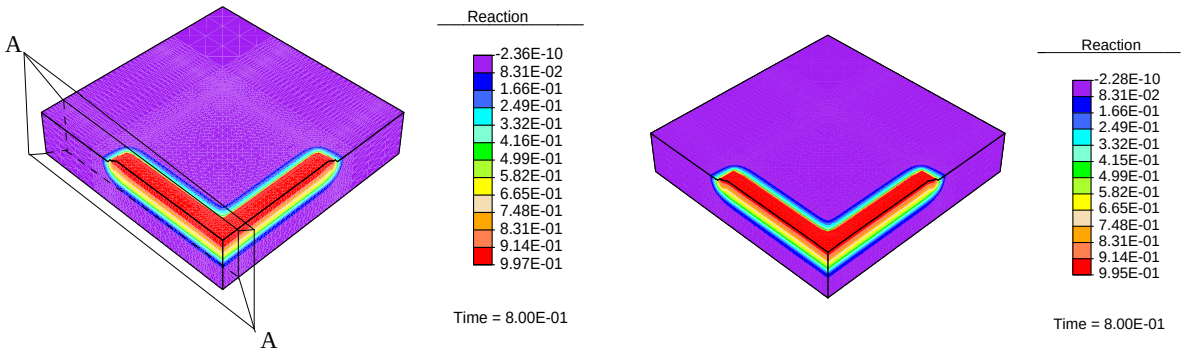

Figure 8. Reaction Contours in the 3-D slab at $\theta = 0.8$.

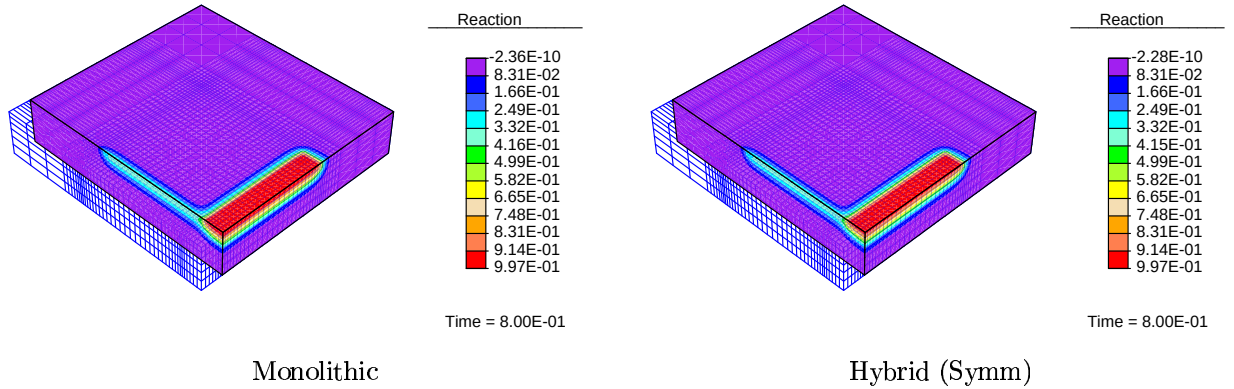

Figure 9. Cross-Section showing Reaction Fronts in the 3-D slab at $\theta = 0.8$.

Scheme	Mono.	Hybrid (Symm.)
CPU time (sec)	5.9825×10^4	1.9142×10^4
ratio	3.12	1.00
Mono. iter.	1702	279
Mech. iter.	–	749
Conc. iter.	–	637
NM	176	33
NS	–	139
Δt_{avg}	4.5×10^{-3}	4.7×10^{-3}

Table IX. Cost Statistics for the 3-D slab with L-Shaped Pattern, $\theta = 0.8$

NM: # of Successful Monolithic Steps, NS: # of Successful Split Steps.

The cost statistics from runs on a Pentium IV, 3.1 GHz, 512MB RAM machine are provided in Table IX. With regard to CPU time, the symmetric hybrid scheme beats the monolithic scheme by a factor of 3.12. The extreme coupling and nonlinearities resulted in an average of 10 Newton iterations per successful step for the monolithic scheme[‖]. On the other hand, the split steps took around 5 iterations for each phase per successful timestep and emerged as the favored choice. Newton failures for the monolithic scheme in the 3-D case, offsets any benefit the monolithic scheme offers (problem size $\sim 4n$) against the split scheme (problem sizes $\sim 3n$ and $\sim n$, in the two phases of the split). The stepsize sequence is shown in Fig.10. The stepsizes vary by an order of magnitude on average for both the monolithic and hybrid schemes. Unlike the 2-D trench example, the split choice is favored for most of the simulation. In fact, the only times the monolithic step is chosen is when the hybrid scheme is forced to update the current cost of a monolithic step. Towards the end of the simulation, when splitting errors start to dominate, the monolithic choice is made.

6. Conclusions

A general framework incorporating error and cost criteria for efficient time stepping of highly nonlinear, strongly coupled problems is developed. In this context, a novel hybrid time stepping scheme is devised and successfully tested on one such highly nonlinear, strongly coupled problem, namely, silylation. The hybrid scheme objectively evaluates the benefit of using time splitting in the broader context of ensuring accuracy, efficiency and robustness. By providing the monolithic alternative in its framework and an algorithm for choosing the best among monolithic and split alternatives, the common drawback of inaccurate results with large stepsizes or inefficient results with small stepsizes for splitting schemes in strong/varying coupling situations is completely removed. Based on numerical results in both 2- and 3-D

[‖]Calculated as 1702/176∼10. Here, 176 denotes only the number of successful steps while 1702 denotes the Newton iterations that include those accrued from failed steps.

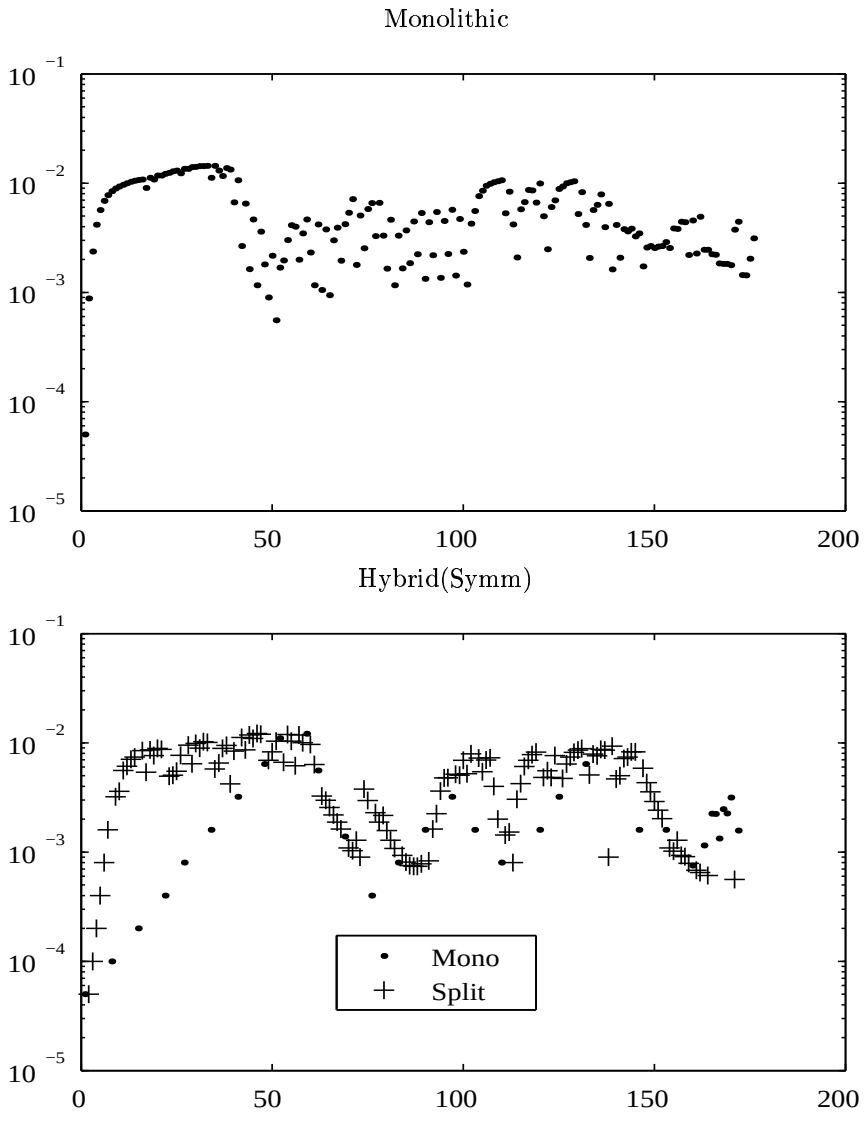

Figure 10. Stepsize Sequence versus Step Number for the L-pattern silylation of the 3-D slab. X-axis: Step #, Y-axis: Log[$\Delta\theta$].

situations, the hybrid scheme is definitely seen to be cost effective–the best one can achieve for a target accuracy.

Although not emphasized in this paper, the hybrid scheme proved to be indispensable for simulating silylation. Numerical simulations have illustrated that strong coupling is necessary for sharp reaction fronts silylating the dry polymer at a constant speed and the accompanying polymer swelling. These features are simply not achievable from a pure uncoupled nonlinear diffusion viewpoint. Although the physically consistent coupled viewpoint has been around, the hybrid scheme has provided the right tools to simulate such a coupled model.

Acknowledgments

The authors wish to acknowledge the invaluable help of Prof. R. L. Taylor in the implementation of the adaptive hybrid scheme in FEAP, a finite element analysis program. The support in part by the National Science Foundation through award CMS–9734121 is also gratefully acknowledged.

Appendix-A: Non-dimensional form of the governing equations

Denoting non-dimensional quantities by $\overline{(\cdot)}$, the non-dimensional physical quantities and governing equations are:

- *Non-dimensional spatial and reference coordinates*

$$\bar{\mathbf{x}} = \mathbf{x}/L, \tag{34}$$

$$\bar{\mathbf{X}} = \mathbf{X}/L, \tag{35}$$

  where L is a characteristic length of the domain.

- *Non-dimensional time*

$$\theta = \frac{B_{max} t}{L^2} \tag{36}$$

  where B_{max} is an estimated mobility maximum over the domain.

- *Non-dimensional Concentration*

$$\bar{M} = c_5 M \tag{37}$$

  where $1/c_5$ is the density of the pure solvent.

- *Non-dimensional Deformation Measures*

$$\bar{\mathbf{F}} = \partial\bar{\mathbf{x}}/\partial\bar{\mathbf{X}} = \mathbf{F} \tag{38}$$

$$\bar{\mathbf{C}} = \bar{\mathbf{F}}^T\bar{\mathbf{F}} = \bar{\mathbf{C}} \tag{39}$$

$$\bar{J} = J \tag{40}$$

- *Non-dimensional Reacted Sites Concentration*

$$\bar{R} = R/R_{max}. \tag{41}$$

- *Non-dimensional Relaxation time*

$$\bar{\tau} = \frac{B_{max}\tau}{L^2}. \tag{42}$$

- *Mixture Stress Equilibrium*

$$\overline{\mathrm{DIV}}[\bar{\mathbf{F}}\bar{\mathbf{S}}] = \mathbf{0}, \tag{43}$$

  where $\bar{\mathbf{S}} = \mathbf{S}/G$ and G has dimensions of an elastic modulus.
- *Viscoelastic Stresses*

$$\frac{d\bar{q}}{d\theta} + \frac{\bar{q}}{\bar{\tau}(M,J)} = \beta\frac{d\bar{p}^{\infty}}{d\theta}, \tag{44}$$

$$\frac{d\bar{\mathbf{Q}}}{d\theta} + \frac{\bar{\mathbf{Q}}}{\bar{\tau}(M,J)} = \alpha\frac{d}{d\theta}[\frac{\partial\tilde{\psi}^{E}}{\partial\tilde{\mathbf{C}}}], \tag{45}$$

  where, $\bar{p}^{\infty} = p^{\infty}/G$ and $\bar{\mathbf{S}}^{\infty}_{DEV} = \mathbf{S}^{\infty}_{DEV}/G$.
- *Total Stress*

$$\bar{\mathbf{S}} = \bar{\mathbf{S}}^{\infty}_{DEV} + \bar{\mathbf{Q}} + \bar{J}\bar{p}\bar{\mathbf{C}}^{-1} \tag{46}$$

- *Chemical Reaction*

$$\frac{d\bar{R}}{d\theta} = \bar{K}_r\frac{(1-\bar{R})\bar{M}}{\bar{J}}, \tag{47}$$

  where, $\bar{K}_r = K_r B_{max}/c_5$ is the normalized rate constant.

Similarly, the operators $\overline{\mathrm{GRAD}}$, $\overline{\mathrm{grad}}$, $\overline{DIV}$ and $\overline{div}$ are defined as derivatives with respect to dimensionless referential and spatial coordinates.

Appendix-B: Symmetric version of the Hybrid scheme

Consider the deviatoric viscous term in the total stress at time t_{n+1}, namely, $2\rho_0 J_{n+1}^{-\frac{2}{3}}\mathrm{DEV}_{n+1}[\mathbf{Q}_{n+1}]$**. The viscous stress $\mathbf{Q}_{n+1}$ is given by:

$$\mathbf{Q}_{n+1} = \underbrace{\frac{\mathbf{Q}_n}{1+\frac{\Delta t}{\tau}} - \frac{2\alpha}{1+\frac{\Delta t}{\tau}}\tilde{\boldsymbol{\nabla}}\tilde{\psi}^{E}\left(\tilde{\mathbf{C}}_n\right)}_{\mathbf{H}_n} + \frac{2\alpha}{1+\frac{\Delta t}{\tau}}\tilde{\boldsymbol{\nabla}}\tilde{\psi}^{E}\left(\tilde{\mathbf{C}}_{n+1}\right). \tag{48}$$

Here, the notation $\tilde{\boldsymbol{\nabla}}\tilde{\psi}^{E}\left(\tilde{\mathbf{C}}_{(.)}\right) = \partial\tilde{\psi}^{E}/\partial\tilde{\mathbf{C}}_{(.)}$ is adopted for showing the argument of the derivative clearly. Taking the differential Δ of the viscous term expressed as a function of

**The other contributions to the total stress lead to symmetric tangent moduli. Therefore, only the viscous term is considered.

$\mathbf{C}_{n+1}$, one obtains:

$$\Delta\left[J_{n+1}^{-\frac{2}{3}}\mathrm{DEV}_{n+1}(\mathbf{Q}_{n+1})\right] = \hat{\mathbb{C}} : \frac{1}{2}\Delta\mathbf{C}_{n+1} + J_{n+1}^{-\frac{2}{3}}\left[\frac{J_{n+1}\Delta t}{\tau^2(1+\frac{\Delta t}{\tau})}\frac{\partial\tau}{\partial J_{n+1}}\mathrm{DEV}_{n+1}(\mathbf{Q}_{n+1})\otimes\mathbf{C}_{n+1}^{-1}\right] : \frac{1}{2}\Delta\mathbf{C}_{n+1} \tag{49}$$

Here, $\hat{\mathbb{C}}$ is a symmetric rank 4 tangent modulus tensor. For the modified Neo-Hookean model, it is given by:

$$\begin{aligned}\hat{\mathbb{C}} = \frac{4\mu^E\alpha J_{n+1}^{-\frac{2}{3}}}{3(1+\frac{\Delta t}{\tau})}\Bigg(&-\mathbf{C}_{n+1}^{-1}\otimes\mathbf{I} - \mathbf{I}\otimes\mathbf{C}_{n+1}^{-1} + \quad \mathrm{tr}\mathbf{C}_{n+1}\mathbb{I}^{\mathbf{C}_{n+1}^{-1}} + \\ &\frac{1}{3}\mathrm{tr}\mathbf{C}_{n+1}\mathbf{C}_{n+1}^{-1}\otimes\mathbf{C}_{n+1}^{-1}\Bigg) - \\ \frac{2J_{n+1}^{-\frac{2}{3}}}{3}\Bigg(&\mathbf{H}_n\otimes\mathbf{C}_{n+1}^{-1} + \mathbf{C}_{n+1}^{-1}\otimes\mathbf{H}_n \\ &- \frac{\mathrm{tr}(\mathbf{H}_n\mathbf{C}_{n+1})}{3}\mathbf{C}_{n+1}^{-1}\otimes\mathbf{C}_{n+1}^{-1} - \frac{\mathrm{tr}(\mathbf{H}_n\mathbf{C}_{n+1})}{2}\left[\mathbb{I}^{\mathbf{C}_{n+1}^{-1}}\right]\Bigg)\end{aligned} \tag{50}$$

In the above equations, $\mathbf{I}$ is the rank 2 identity tensor while the components of $\mathbb{I}^{\mathbf{C}_{n+1}^{-1}}$ (dropping the subscript $n+1$) are given by $\mathbb{I}^{\mathbf{C}^{-1}}_{ABCD} = \left(\mathbf{C}^{-1}_{AC}\mathbf{C}^{-1}_{BD} + \mathbf{C}^{-1}_{AD}\mathbf{C}^{-1}_{BC}\right)/2$.

From the above derivation, the dependence of $\tau = \tau(M_n, J_{n+1})$ on J_{n+1} in the deformation phase leads to an unsymmetric tangent modulus and subsequently an unsymmetric tangent stiffness. Without losing first order accuracy, one can simply set $\tau = \tau(M_n, J_n)$ and eliminate the 2^{nd} (unsymmetric) term in Eqn. (49). This approximation is made in the symmetric version of the hybrid scheme leading to a symmetric tangent stiffness in the deformation phase of a splitting step. In the unsymmetric hybrid version, the original unsymmetric tangent modulus is utilized in the deformation phase of a splitting step.

Appendix-C: Further Implementation Details

In the actual implementation of the spatial discretization of the mass balance equation and stress equilibrium equations, two special issues have to be addressed. Firstly, the presence of the $c_2\bar{J} + c_4 - \bar{M}$ term in the swelling pressure, $\bar{p}_s$ behaves as a singularity as $\bar{M}$ approaches $c_2\bar{J} + c_4$ making the mixture nearly incompressible. Therefore, ill-effects of incompressibility on the numerical scheme have to be addressed. Secondly, the mass matrix $\mathbf{M}$ is the so-called consistent mass matrix which leads to an oscillatory solution for the activity field (and in turn the concentration) near the sharp fronts. These oscillations are unphysical and we want to avoid them.

The first issue is handled by using mixed pressures $\widehat{p}$ which are calculated in terms of mixed

activity $\widehat{A}$ and mixed Jacobian determinant $\widehat{J}$ as follows. The equations are recalled from [17].

$$\text{Mixed Jacobian: } \int_{\bar{\Omega}} (\widehat{J} - J)\delta\widehat{J}, d\mathbf{x} = 0, \tag{51a}$$

$$\text{Mixed Activity: } \int_{\bar{\Omega}} (\widehat{A} - A)\delta\bar{A}\, d\mathbf{x} = 0, \tag{51b}$$

$$\text{Mixed Pressure: } \int_{\bar{\Omega}} (\widehat{P} - P(\widehat{A}, \widehat{J}))\delta\widehat{P}\, d\mathbf{x} = 0. \tag{51c}$$

In Eqns. (51a), (51b) and (51c), mixed Jacobian, mixed activity and the mixed pressures are interpolated as piecewise constants within each element. Consequently, these mixed quantities can be obtained elementwise for each element. Further motivation for the specific mixed equations used here can be provided through a three-field Hu-Washizu interpretation by Simo et al. [30] for the nearly incompressible purely mechanical problem.

The second issue is handled by considering a mass lumping technique using the mixed Jacobian determinant $\widehat{J}$ and the nodal activity $A^{(.)}$.

$$\mathbf{M} = \mathop{\mathbf{A}}_{e=1}^{n_{el}} \mathbf{m}^{(e)}_{[N_{en} \times N_{en}]} \tag{52}$$

$$\mathbf{m}^{(e)}_{(I,J)} = \frac{\partial \bar{M}(A^J_{n+1}, \widehat{J}_{n+1})}{\partial A}\delta^{IJ} \int_{\mathbf{\Omega}_e} N^I d\bar{\mathbf{x}}. \tag{53}$$

REFERENCES

1. A. S. Argon, R. E. Cohen, and A. C. Patel. A mechanistic model of Case II diffusion of a diluent into a glassy polymer. *Polymer*, 40:6991–7012, 1999.
2. F Armero. Formulation and finite element implementation of a multiplicative model of coupled pore-plasticity at finite strains under fully saturated conditions. *Computer Methods in applied Mechanics and Engineering*, 171:205–241, 1999.
3. F. Armero and J. C. Simo. A new unconditionally stable fractional step method for nonlinear coupled thermomechanical problems. *International Journal for Numerical Methods in Engineering*, 35:737–756, 1992.
4. K. Arshak, M. Mihov, A. Arshak, and D. McDonagh. Top surface imaging lithography processes for i-line resists using liquid-phase silylation. volume 2 of *Proceedings of the 23rd International Conference on Microelectronics*, pages 503–508, Yugoslavia, May 2002.
5. K. Arshak, M. Mihov, A. Arshak, D. McDonagh, M. Pomeroy, and M. Campion. PRIME process with Shipley SPR505A resist - simulations and experiments. *Microelectronic Engineering*, 61:783–792, Jul 2002.
6. L. S. J. Bell and P. J. Binning. A split operator approach to reactive transport with the forward particle tracking eulerian lagrangian localized adjoint method. *Advances in water resources*, 23:467–492, 2004.
7. K E Brenan, S L Campbell, and L R Petzold. *Numerical solution of initial-value problems in differential-algebraic equations*. Elsevier Science Pub. Co., North-Holland, New York, 1989.
8. R. G. Carbonell and G. C. Sarti. Coupled deformation and mass-transport processes in solid polymers. *Industrial and Engineering Chemistry Research*, 29:1194–1204, 1990.
9. N N Carlson and K. Miller. Design and application of a gradient-weighted moving finite element code I: In one dimension. *SIAM Journal of Scientific Computing*, 19:728–765, 1998.
10. P. Causin, M. Restelli, and R. Sacco. A simulation system based on mixed-hybrid finite element analysis for thermal oxidation in semiconductor technology. *Computer Methods in Applied Mechanics and Engineering*, 193:3687–3710, 2004.
11. J. H. Choi and I. Lee. Finite element analysis of transient thermoelastic behaviors in disk brakes. *Wear*, 1–2:47–58, Jul 2004.

12. E. Croffie. Moving boundary models and methods for deep submicron resist process simulation, Report No. UCB/ERL M99/26. Technical report, Electronics Research Laboratory, College of Engineering, U.C. Berkeley, 1999.
13. E L Cussler. *Diffusion, Mass Transfer in Fluid Systems.* Cambridge University Press, New York, 1984.
14. D. Dureisseix, P. Ladeveze, and B. A. Schrefler. A LATIN computational strategy for multiphysics problems: application to poroelasticity. *International Journal for Numerical Methods in Engineering*, 56:1489–1510, March 2003.
15. E. Ellsiepen and S. Hartmann. Remarks on the interpretation of current non-linear finite element analysis as differential-algebraic equations. *International Journal for Numerical Methods in Engineering*, 51:679–707, 2001.
16. S. Govindjee and J. C. Simo. Coupled stress-diffusion: Case II. *Journal of the Mechanics and Physics of Solids*, 41:863–887, 1993.
17. S. Govindjee. *Physical and Numerical Modelling in Filled Elastomeric Systems.* PhD thesis, Stanford University, 1991.
18. E. Hairer and G. Wanner. *Solving ordinary differential equations II: Stiff and Differential-Algebraic problems.* Springer-Verlag, New York, 1993.
19. M. A. Hartney. Modeling of positive-tone silylation processes for 193-nm lithography. *Journal of Vaccuum Science and Technology, B*, 11:681–687, 1993.
20. T. J. R. Hughes. *The Finite Element Method: Linear Static and Dynamic Finite Element Analysis.* Dover Publications, Inc., New York, 2000.
21. D. A. Knoll and D. E. Keyes. Jacobian-free newton-krylov methods: A survey of approaches and applications. *Journal of Computational Physics*, 193:357–397, Jan 2004.
22. D. Kuhl, F. Bangert, and G. Meschke. Coupled chemo-mechanical deterioration of cementitious materials–part II: Numerical methods and simulation. *International Journal of Solids and Structures*, 41:41–67, Jan 2004.
23. J D Lambert. *Numerical Methods for Ordinary Differential Equations: The initial value problem.* John Wiley and Sons, New York, 1993.
24. D. Lanser and J. G. Verwer. Analysis of operator splitting for advection-diffusion-reaction problems in air pollution modelling. *Journal of Computational and Applied Mathematics*, 111:201–216, 1999.
25. R. W. Lewis and B. A. Schrefler. *The finite element method in static and dynamic deformation and consolidation of porous media.* Wiley Press, New York, 2 edition, 1998.
26. K Miller. Class notes for MATH 228A, U.C. Berkeley. Unpublished, 1997.
27. M. Sanopoulou, D. F. Stamatialis, and J. H. Petropoulos. Investigation of case II diffusion behavior. 1. Theoretical studies based on the relaxation dependent solubility model. *Macromolecules*, 35:1012–1020, 2002.
28. B. A. Schrefler, L. Simoni, and E. Turska. Standard staggered and staggered newton schemes in thermo-hydro-mechanical problems. *Computer Methods in Applied Mechanics and Engineering*, 144:93–109, 1997.
29. J. R. Sheats and B. W. Smith, editors. *Microlithography Science and Technology.* Marcel Dekker, 1998.
30. J. C. Simo, R. L. Taylor, and K. S. Pister. Variational and projection methods for the volume constraint in finite deformation elasto-plasticity. *Computer Methods in Applied Mechanics and Engineering*, 51:177–208, 1985.
31. S. W. Sloan and A. J. Abbo. Biot consolidation analysis with automatic time stepping and error control part 1: Theory and implementation. *International Journal for numerical and analytical methods in geomechanics*, 23:467–492, 1999.
32. J. Stoer and R. Bulirsch. *Introduction to numerical analysis.* Springer, New York, 2002.
33. G Strang. On construction and comparison of difference schemes. *SIAM Journal on Numerical Analysis*, 5:506–517, 1968.
34. N L Thomas and A H Windle. Case-II swelling of PMMA sheet in methanol. *Journal of Membrane Science*, 3:337–342, 1978.
35. N L Thomas and A H Windle. A theory of case-II diffusion. *Polymer*, 23:529–542, 1982.
36. E. Turska and B. A. Schrefler. On convergence conditions of partitioned solution procedures for consolidation problems. *Computer Methods in Applied Mechanics and Engineering*, 106:51–63, 1993.
37. P. K. Vijalapura and S. Govindjee. Numerical simulation of coupled-stress case II diffusion in one dimension. *Journal of Polymer Science Part B: Polymer Physics*, 41:2091–2108, 2003.
38. P. K. Vijalapura, J. A. Strain, and S. Govindjee. Fractional step methods for index-1 differential algebraic equations. *Journal of Computational Physics*, 203:305–320, 2005.
39. P. K. Vijalapura. *Numerical Simulation of Solvent Diffusion and Reaction in Deforming Polymers: Applications to Microlithfography.* PhD thesis, University of California, Berkeley, 2004.
40. P. K. Vijalapura. Numerical simulation of Case II diffusion in one dimension. Technical Report UCB/SEMM-2002/07, University of California, Berkeley, 2002.
41. W. L. Wood. *Practical time-stepping schemes.* Oxford Applied Mathematics and Computing Science

series. Oxford University Press, 1990.
42. O. C. Zienkiewicz, D. K. Paul, and A. H. C. Chan. Unconditionally stable staggered solution procedure for soil pore fluid interaction problems. *International Journal for Numerical Methods in Engineering*, 26:1039–1055, 1988.
43. T. I. Zohdi. An adaptive-recursive staggering strategy for simulating multifield coupled processes in micro-heterogeneous solids. *International Journal of Numerical Methods in Engineering*, 53:1511–1532, 2002.
44. T. I. Zohdi. Modeling and simulation of a class of coupled thermo-chemo-mechanical processes in multiphase solids. *Computer Methods in Applied Mechanics and Engineering*, 193:679–699, 2004.